The Astrophysical Journal, 918:87 (12pp), 2021 September 10 https://doi.org/10.3847/1538-4357/ac0e9e
© 2021. The American Astronomical Society. All rights reserved.

Advective Accretion onto a Nonspherical Accretor in White Dwarf and Neutron Star Binaries: A New Scenario of Shock Formation

Sudeb Ranjan Datta[1], Prasun Dhang[2,3], and Bhupendra Mishra[4]
[1] Dept. of Physics, Indian Institute of Science, Bangalore-560012, India; sudebd@iisc.ac.in
[2] Institute for Advanced Study, Tsinghua University, Beijing-100084, People's Republic of China
[3] Department of Astronomy, Tsinghua University, Beijing-100084, People's Republic of China
[4] Los Alamos National Lab, Los Alamos, NM 87545, USA
Received 2020 November 30; revised 2021 June 16; accepted 2021 June 16; published 2021 September 15

Abstract

Numerous studies on hydrodynamics of the Keplerian as well as the sub-Keplerian accretion disk around a compact object (e.g., white dwarf (WD), neutron star (NS), or a black hole) have attempted to explain the observed UV, soft, and hard X-ray spectra. Although, when the compact object (e.g., a WD or an NS) has a finite surface, its rapid rotation, the stellar magnetic field could cause deformation of the spherical symmetry. Earlier studies on the Keplerian disk showed that a deviation from the spherical symmetry of the compact object could affect the observed light curve and spectra at high frequencies. Here, we have explored the effect of the nonspherical nature of a compact object on the hydrodynamics of an optically thin, geometrically thick sub-Keplerian advective flow. We find that due to the nonspherical shape of the central accretor, there is a possibility to trigger Rankine–Hugoniot shock in the sub-Keplerian advective flow close to the accretor without considering any general relativistic effect or presence of the hard surface of the star. Our results are more relevant for accretion onto a WD as hardly any general relativistic effect will come into the picture. We propose that some observational features, e.g., high significance of fitting the spectra with multi-temperature plasma models rather than single-temperature models, and variable efficiency of X-ray emission (X-ray luminosity in comparison with the optical and UV luminosity of the disk) in nonmagnetic cataclysmic variables can be explained by the presence of a shock in the sub-Keplerian advective flow.

Unified Astronomy Thesaurus concepts: High energy astrophysics (739); Cataclysmic variable stars (203); White dwarf stars (1799); Accretion (14); Shocks (2086)

1. Introduction

The physics of accretion disks has remained an open area of research over the last few decades. Despite great progress in our understanding, we still need better theoretical model to shed light on recent observations. Generally, there are three theoretical models of accretion disks: (i) geometrically thin and optically thick Keplerian disk (Shakura & Sunyaev 1973), (ii) geometrically thick and optically thin advective flows (Chakrabarti 1989; Narayan & Yi 1994), and (iii) geometrically and optically thick slim disks (Abramowicz et al. 1988). Various accreting sources often show variability in observed luminosity and could change the geometrical shape of accretion disks.

The presence of a geometrically thick and optically thin advective flow is essential to explain hard X-rays and soft γ-rays from accreting systems like neutron stars (NSs) and black holes (BHs; Chakrabarti & Titarchuk 1995; Narayan et al. 1998; Yuan et al. 2005). Due to the advective properties of thick flows, thermal energy generated due to viscous dissipation gets advected into central object before it can escape vertically from the disk surface. The advection of thermal energy in such geometrically thick hot flows plays an important role in stabilization against thermal instability. Flow remains hot, optically thin, geometrically thick, and is able to give higher energy photons (Narayan & Yi 1994, 1995). On the other hand in a Keplerian, optically thick, geometrically thin Shakura–Sunyaev disk (SSD; Novikov & Thorne 1973; Shakura & Sunyaev 1973; Pringle 1981) emission of multi-temperature blackbody radiation is sufficient to balance the viscous heating. The resultant emission is observed in soft X-rays and is of higher luminosity. To explain the observed spectra, two-component accretion flow is also invoked (Chakrabarti & Titarchuk 1995; Chakrabarti 1996; Chatterjee et al. 2018).

Several observations show that like BH and NS systems, accreting nonmagnetic white dwarf (WD) systems (cataclysmic variables; CVs) also produce hard X-rays in all types of source states (and not soft X-rays as would be expected in high accretion rate states), the origin of which is interpreted to be connected to the presence of a radiatively inefficient (advective) accretion flow (Balman et al. 2014; Godon et al. 2017; Balman 2020, and references therein). However, Pringle & Savonije (1979) proposed the possibility of emission of hard X-rays from nonmagnetic CVs under low accretion rate depending on the effectiveness of a shock in a Keplerian SSD. For a detailed discussion on the presence of advective flows in nonmagnetic CVs see Section 5.3.

One crucial difference between the advective flow around the NS or the BH and that onto a WD is that protons are unable to transfer their energy to electrons and two temperature plasma comes into the picture for the former case (Narayan & Yi 1995; Rajesh & Mukhopadhyay 2010), while for the latter, the temperature of the protons and the electrons remains almost the same; however, see Section (5.4) (Frank et al. 2002; Medvedev & Menou 2002). Therefore, radiatively inefficient advective flow in CVs can be treated as a single-temperature fluid (Chakrabarti 1989; Narayan & Popham 1993; Popham& Narayan 1995; Chakrabarti 1996). For this preliminary model, we assume here that the disk is completely ionized.

It is probable that presence of the stellar rotation, strong stellar magnetic field and continuous accretion can change the spherical shape of the central accretor (Ostriker & Bodenheimer 1968; Ostriker & Hartwick 1968; Shapiro & Teukolsky 1983; Komatsu et al. 1989; Haskell et al. 2008; Das & Mukhopadhyay 2015; Subramanian & Mukhopadhyay 2015). One first-order generalization of spherical shape is the Maclaurin spheroid (MS; Chandrasekhar 1969). Deviation from the spherical symmetry of an accreting source leads to a change in the gravitational force exerted on a test particle orbiting very close to it and could alter the dynamics of the accretion flow. Despite such an effect of gravity, the gravitational potential of an MS remains Newtonian and we do not consider any general relativistic (GR) effects for this work.

There are already a few theoretical studies on orbits around an MS (Amsterdamski et al. 2002; Kluźniak & Rosińska 2013) and SSDs around an MS accretor (Mishra & Vaidya 2015). These studies showed the emergence of many new features in the accretion flow just because of the deformation of the shape of the compact object. In this paper, we study the sub-Keplerian advective flow around an NS and a WD considering the accretor to be an MS. To do a preliminary analysis, we consider a low angular momentum (sub-Keplerian) inviscid flow. It is convenient to assume such low value of angular momentum in modeling sub-Keplerian advective flow and its characteristic properties (Chakrabarti 1989; Das et al. 2001; Palit et al. 2019). However, it must be emphasized that our reported model in this article is primarily applicable to WDs since GR effects do not play a crucial role in accretion disks around such a compact object. The importance of our reported theory could also be realized to describe accretion flow around a rapidly rotating NS but not very precisely without including all the GR effects. Therefore, in the rest of the article, we primarily focus on accretion disks around WDs rather than NSs. Although inclusion of GR effects will change the properties of the flow and will change the parameter space for our model to be applicable, we expect the qualitative picture will remain same.

An inner sonic point (see Section 2) does not exist for accretion onto a spherical Newtonian accretor. That is why shock cannot be realized within the sub-Keplerian advective flow around a spherical Newtonian accretor unless there is the presence of a hard surface (Dhang et al. 2016) or GR correction in gravitational potential is taken into account (Chakrabarti 1989, 1996; Mukhopadhyay 2002; Dihingia et al. 2020). For accretion onto a WD, to the best of our knowledge, we are reporting for the first time that formation of a shock is possible in the appropriate parameter space due to the deformed shape of the accretor. To some extent, the shocks can explain the scenarios where the hard X-ray emission components that are predominantly detected both in the quiescence and outburst in the inner disk and the X-ray emitting region. There seems to be a few detections of the soft X-ray regime during outbursts (i.e., state transition to high state) and no detection of soft X-ray emission in persistent high state CVs. This suggests that an optically thick standard boundary does not form (see discussions in Balman et al. (2014), Balman (2020), section 2.3, and references therein). The shocks we calculate, can explain the detected hard X-ray emissions in nonmagnetic CVs when the different parameters of the central accretor and of the flow are suitable for the shocks to occur.

The plan of the paper is as follows. In Section 2, we present the formalism we follow. We analyze the parameter space for advective accretion flow in Section 3. In Section 4, we present the hydrodynamics of flow around an NS as well as a WD. We discuss the possible connection of our work to observations in Section 5. Finally we conclude in Section 6.

2. A General View of the Formalism

We use a standard approach (e.g., see Chakrabarti 1989; Mukhopadhyay 2003) to investigate the inviscid accretion flow around a compact star (e.g., an NS or a WD) whose gravity can be described by the gravitational force due to an MS. Specifically, we want to study the effects of deformation (may be due to rotation of the star or due to the intrinsic stellar magnetic field).

To obtain the flow variables, we solve conservation of mass (mass continuity equation) and momentum (radial momentum balance equation) as given below:

$$\frac{d}{dr}(r\Sigma v) = 0, \tag{1}$$

$$v\frac{dv}{dr} + \frac{1}{\rho}\frac{dP}{dr} - \frac{l^2}{r^3} + F(r) = 0, \tag{2}$$

where $\Sigma = 2\rho(r)h(r)$ is the vertically integrated surface density and $F(r)$ is the gravitational force for an MS. Here, $\rho(r)$ is the density and $h(r)$ is the half thickness of the disk. Unless otherwise stated, all the radial distances in this paper are in units of GM/c^2, where M is the mass of the MS, G is the gravitational constant, and c is the speed of light. The velocity v is in units of c and specific angular momentum l is in units of GM/c.

Along with Equations (1) and (2), we use the polytropic equation

$$P = K\rho^{\gamma} \tag{3}$$

to describe the equation of state, where γ is the adiabatic index. The gravitational force due to MS at the equatorial plane is

$$\begin{aligned} F(r) &= \Omega^2 r \\ &= 2\pi G\rho_*(1-e^2)^{1/2}e^{-3}(\gamma_r - \cos\gamma_r \sin\gamma_r)r, \end{aligned} \tag{4}$$

where e is the eccentricity and ρ_* is the density of MS, taken to be uniform. $\gamma_r = \sin^{-1}(ae/r)$, a is the semimajor axis of MS.

In dimensionless units, force takes the form

$$F(r) = 1.5(ae)^{-3}(\gamma_r - \cos\gamma_r \sin\gamma_r)r \tag{5}$$

and $h(r)$ can be found from the vertical equilibrium equation as

$$h(r) = c_s r^{1/2} F^{-1/2}, \tag{6}$$

where $c_s = \sqrt{\gamma p/\rho}$ is the sound speed. Unless mentioned specifically, we use $\gamma = 4/3$.

Now, combining Equations (1) and (2) we get

$$\frac{dv}{dr} = \left[\frac{l^2}{r^3} - F(r) + \frac{c_s^2}{\gamma+1}\left(\frac{3}{r} - \frac{1}{F}\frac{dF}{dr}\right)\right] \Bigg/ \left[v - \frac{2c_s^2}{(\gamma+1)v}\right]. \tag{7}$$

Far away from the accretor, the radial velocity v is small and subsonic. As the flow approaches the accretor, v increases and

in principle can exceed the local sound speed c_s, i.e., can become supersonic. This implies that at a critical radius r_c, the denominator of Equation (7) becomes zero, i.e., at r_c, v becomes equal to $\sqrt{2/(\gamma+1)}c_s$. Though $v \neq c_s$ at $r = r_c$, historically, a standard trend in the literature is to write subsonic and supersonic flow before and after the critical point (r_c). We follow the same traditional nomenclature in this work also. For a realistic flow, the presence of a non-divergent velocity gradient leads to the requirement that the numerator of Equation (7) also vanishes so that we can use L'Hospital rule to have a definite $\frac{dv}{dr}|_c$. Using L'Hospital's rule, the slope for velocity at the critical point becomes

$$\left.\frac{dv}{dr}\right|_c = -\frac{B + \sqrt{B^2 - 4AC}}{2A}, \tag{8}$$

where

$$A = 1 + \frac{2c_{sc}^2}{(\gamma+1)v_c^2}\left[1 + 2\left(\frac{\gamma-1}{\gamma+1}\right)\right], \tag{9}$$

$$B = \frac{4c_{sc}^2(\gamma-1)}{v_c(\gamma+1)^2}\left(\frac{3}{r_c} - \frac{1}{F_c}\left.\frac{dF}{dr}\right|_c\right), \tag{10}$$

$$C = \frac{3l^2}{r_c^4} + \left.\frac{dF}{dr}\right|_c + \frac{c_{sc}^2(\gamma-1)}{(\gamma+1)^2}\left[\frac{3}{r_c} + \frac{1}{F_c}\left.\frac{dF}{dr}\right|_c\right]^2 - \frac{c_{sc}^2}{\gamma+1}\left[\left(\frac{1}{F_c}\left.\frac{dF}{dr}\right|_c\right)^2 - \frac{1}{F_c}\left.\frac{d^2F}{dr^2}\right|_c - \frac{3}{r_c^2}\right]. \tag{11}$$

Equating the denominator and the numerator of Equation (7) to zero, we get the Mach number

$$\mathcal{M}_c = \frac{v_c}{c_{sc}} = \sqrt{\frac{2}{\gamma+1}} \tag{12}$$

and sound speed

$$c_{sc} = \sqrt{(\gamma+1)\left(F_c - \frac{l^2}{r_c^3}\right)\Big/\left(\frac{3}{r_c} - \frac{1}{F_c}\left.\frac{dF}{dr}\right|_c\right)} \tag{13}$$

at the critical point r_c. Now integrating Equations (1) and (2), we can write the energy and entropy of the flow at the critical point as

$$E_c = \frac{2\gamma}{(\gamma-1)}\left[\left(F_c - \frac{l^2}{r_c^3}\right)\Big/\left(\frac{3}{r_c} - \frac{1}{F_c}\left.\frac{dF}{dr}\right|_c\right)\right] + V_c + \frac{l^2}{2r_c^2} \tag{14}$$

and

$$\dot{\mu}_c = (\gamma K)^n \dot{M} = r_c^{3/2} F_c^{-1/2} (\gamma+1)^{q/2} \times \left[\left(F_c - \frac{l^2}{r_c^3}\right)\Big/\left(\frac{3}{r_c} - \frac{1}{F_c}\left.\frac{dF}{dr}\right|_c\right)\right]^{\gamma/(\gamma-1)}, \tag{15}$$

where $V_c = (\int F dr)|_c$, $q = (\gamma+1)/[2(\gamma-1)]$ and $n = 1/(\gamma-1)$. Here $\dot{\mu}$ carries the information of entropy. For a non-dissipative system E remains constant throughout the flow. Here an important point to note is that formation of a shock enhances the entropy which changes the value of "K", which finally changes the value of $\dot{\mu}_c$. Therefore, due to mass continuity $\dot{M}$ remains same throughout the flow, while the formation of a shock increases the value of $\dot{\mu}_c$ due to the increment of entropy.

Figures 1 and 2 show the variation of energy at critical point (E_c) with the position of the critical point (r_c) for different l and ae values, respectively, for the parameters applicable to a typical NS and WD. As we investigated here non-dissipative flow, fixing the energy at a critical point will fix the energy of the flow. The horizontal lines in Figures 1 and 2 indicate the constant energy of the flow. It is clear that depending on E_c, the locations of the critical points as well as the number of critical points also vary.

This opens up another possibility of formation of Rankine–Hugoniot shock (Landau 1987) in the flow. If we generalize the conditions to form a shock in the accretion disk given by Chakrabarti 1989 for any compact object, we get

$$\frac{1}{2}\mathcal{M}_+^2 c_{s,sh+}^2 + n c_{s,sh+}^2 = \frac{1}{2}\mathcal{M}_-^2 c_{s,sh-}^2 + n c_{s,sh-}^2, \tag{16}$$

$$\frac{c_{sh+}^{\nu}}{\dot{\mu}_+}\left(\frac{2\gamma}{3\gamma-1} + \gamma\mathcal{M}_+^2\right) = \frac{c_{sh-}^{\nu}}{\dot{\mu}_-}\left(\frac{2\gamma}{3\gamma-1} + \gamma\mathcal{M}_-^2\right), \tag{17}$$

$$\dot{\mu}_+ > \dot{\mu}_-, \tag{18}$$

where

$$\dot{\mu} = \mathcal{M} c_s^{2(n+1)} \frac{r_s^{3/2}}{\sqrt{F(r_s)}}. \tag{19}$$

Here, the subscript "sh" indicates the shock, "$-$" and "$+$" subscripts indicate before and after the shock. $\mathcal{M}$ denotes the Mach number of the fluid and exponent of c_s in Equation (17) is $\nu = (3\gamma\text{-}1)/(\gamma\text{-}1)$. Equation (18) indicates the natural choice of formation of shock as entropy increases after the shock. Combining Equations (17) and (19), we get the shock invariant quantity as

$$SIQ = \frac{[2/\mathcal{M}_+ + (3\gamma-1)\mathcal{M}_+]^2}{\mathcal{M}_+^2(\gamma-1)+2} = \frac{[2/\mathcal{M}_- + (3\gamma-1)\mathcal{M}_-]^2}{\mathcal{M}_-^2(\gamma-1)+2}. \tag{20}$$

If conditions (16), (18), and (20) are satisfied simultaneously by the flow, then shock will form in an accretion disk. Though actual values will vary from source to source, due to this shock within advective flow, typically the radial velocity is almost halved. From mass continuity, due to decrement in radial velocity, the density doubles in the post-shock region, which is supposed to enhance the cooling in comparison with the pre-shock flow.

3. Analysis of Parameter Space

In this section, we discuss the dependence of flow properties on different parameters such as eccentricity (e), radius of the central accretor (a), and specific angular momentum of the flow (l). Figure 1 shows how the variation of specific angular momentum of the flow changes the number as well as the location of critical points (Chakrabarti 1989) for fixed values of energy E_c and ae. For example, if we fix $ae = 3.0$ (3540.0 for WD case) as well as the energy of the flow at 0.029 (2.0×10^{-5}), then for $l = 1.65$ ($l = 59.0$) there are four critical points (where the horizontal line of value 0.029 (2.0×10^{-5}) cuts the E_c versus r_c curves). The outer most critical point is an

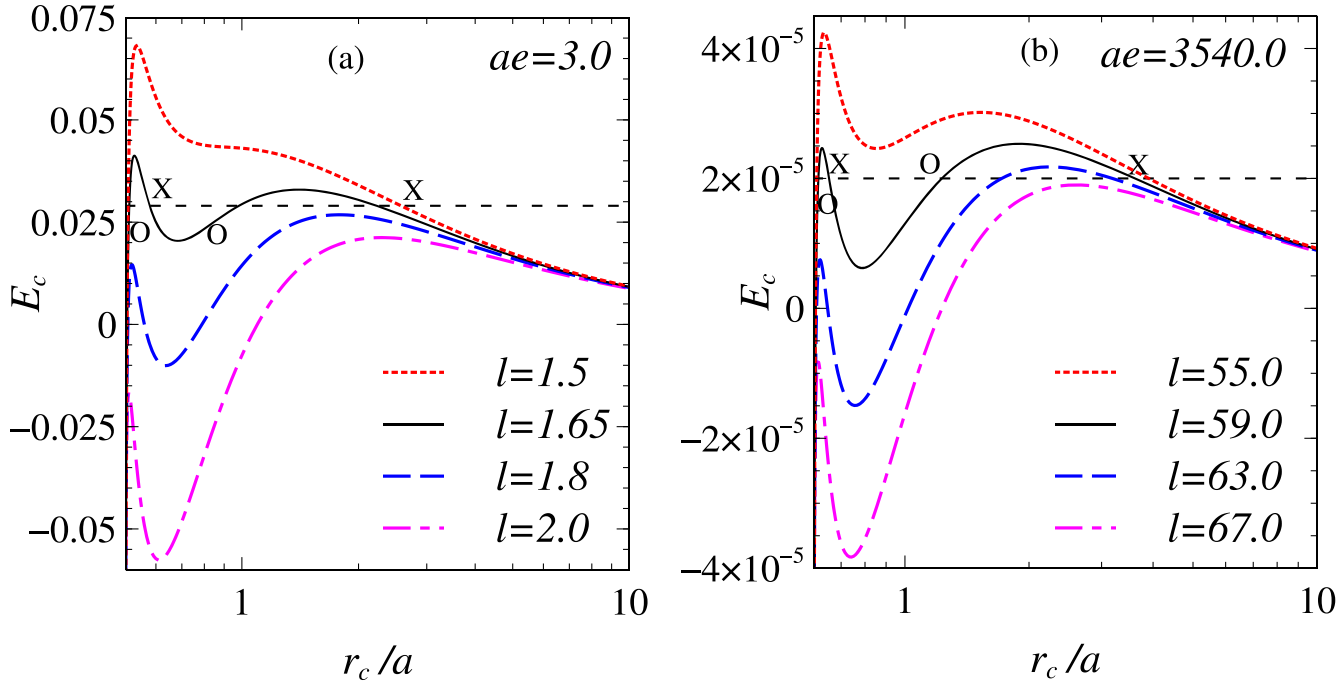

Figure 1. Variation of energy as a function of the critical point location for various values of specific angular momentum (l). Left panel (a) is for parameters for a typical NS. ae is fixed at 3.0 where a and e are assumed to be 6.0 and 0.5, respectively. The horizontal line indicates constant energy of 0.029. Right panel (b) is for a typical WD. ae is fixed at 3540.0, where a and e are assumed to be 5900.0 and 0.6, respectively. The horizontal line indicates a constant energy of 2.0×10^{-5}. Adiabatic index $\gamma = 4/3$. Different types of critical points are marked in the figure. The x-axis values are presenting the critical point location in terms of the semimajor axis (a) of the compact object.

"X" type critical point (slope of E_c versus r_c curve is negative). As we move inside, next critical points are "O" type, "X" type, and "O" type, respectively. Chakrabarti 1990 discusses critical points and their types in detail. For the present purpose it is sufficient to state that X type critical points are responsible for successful accretion. So, our current interest lies in the outer and inner X type critical points. Hereafter, we indicate these two X type critical points as outer and inner critical points. Changing the specific angular momentum of the flow will change E_c of the flow according to Equation (14) as shown by the different curves in Figure 1. Now, for a specific case, the energy of the flow will be fixed for an inviscid flow, which is indicated as a straight line in Figure 1. Therefore, for a particular value of E_c (0.029 for a typical NS and 2.0×10^{-5} for a typical WD) and ae (3.0 for a typical NS and 3540.0 for a typical WD), only a definite range of specific angular momentum ($l \sim$1.6–1.7 for accretion onto a typical NS and $l \sim$58.0–59.0 for accretion onto a typical WD) can give rise to simultaneous occurrence of outer and inner critical points, which is shown in Figure 1. For other l values, with the same E_c and ae, there are different possibilities of occurrence of one X type and one O type, or one X type, or no X type critical point. The consequence of different possibilities is discussed in detail in Chakrabarti (1990). However, our current interest lies in the possibility of shock in the flow, which is possible only when two X type critical points are present simultaneously.

If the angular momentum is low enough, the centrifugal barrier is unable to create any characteristic feature in the flow i.e., occurrence of multiple X type critical points is not possible and flow is smoothly accreted by the accretor. This indicates that due to gradual decrement of specific angular momentum (l), the flow becomes Bondi-like (Bondi 1952) as angular momentum is unable to affect the flow. It is clear from Figure 1 for $l \leqslant 1.5$ in the case of an NS and $l \leqslant 52.0$ in the case of a WD, the flow becomes Bondi-like for our chosen parameter space as E_c increases monotonically with decreasing r_c due to disappearance of an effective centrifugal barrier. It should be mentioned that the presence of both outer and inner critical points is necessary for the shock in the flow to be probable (Chakrabarti 1989).

Next, we show how the change in eccentricity and radius affects critical point analysis. Treating the central accretor as MS, the fundamental difference is coming through the gravitational force it is applying on the test particle (Equation (5)) instead of a spherical accretor. As this force does not involve a and e separately, changing the value of the product of a and e only affects the results, not the individual values of a and e. Figure 2 shows the E_c versus r_c plots for different values of ae and a fixed l. Figure 2 shows that for a fixed E_c (0.029 for a typical NS and 2.0×10^{-5} for a typical WD) and l (1.65 for accretion onto a typical NS and 59.0 for accretion onto a typical WD), a small range of ae ($\sim$2.976–3.018 for the NS and $\sim$3451.5–3599.0 for the WD) can make the shock possible, as in Figure 1, which shows the range of l to make the shock happen. These two figures together indicate that when a flow with fixed energy accretes into a suitable accretor (appropriate value of ae) with a suitable specific angular momentum value, shock will occur. One set of values of different parameters suitable for shock for an NS having $a = 6.0$ and for a WD having $a = 5900.0$ is tabulated in Table 1.

Equation (5) indicates that for a realistic $F(r)$, $r \geqslant ae$. Therefore, while doing a parameter space survey, we restrict to the limit $r \geqslant ae$ value. However, when we present the hydrodynamics of the accretion flow in the next section, we assume that disk truncates at the surface of the star of radius a.

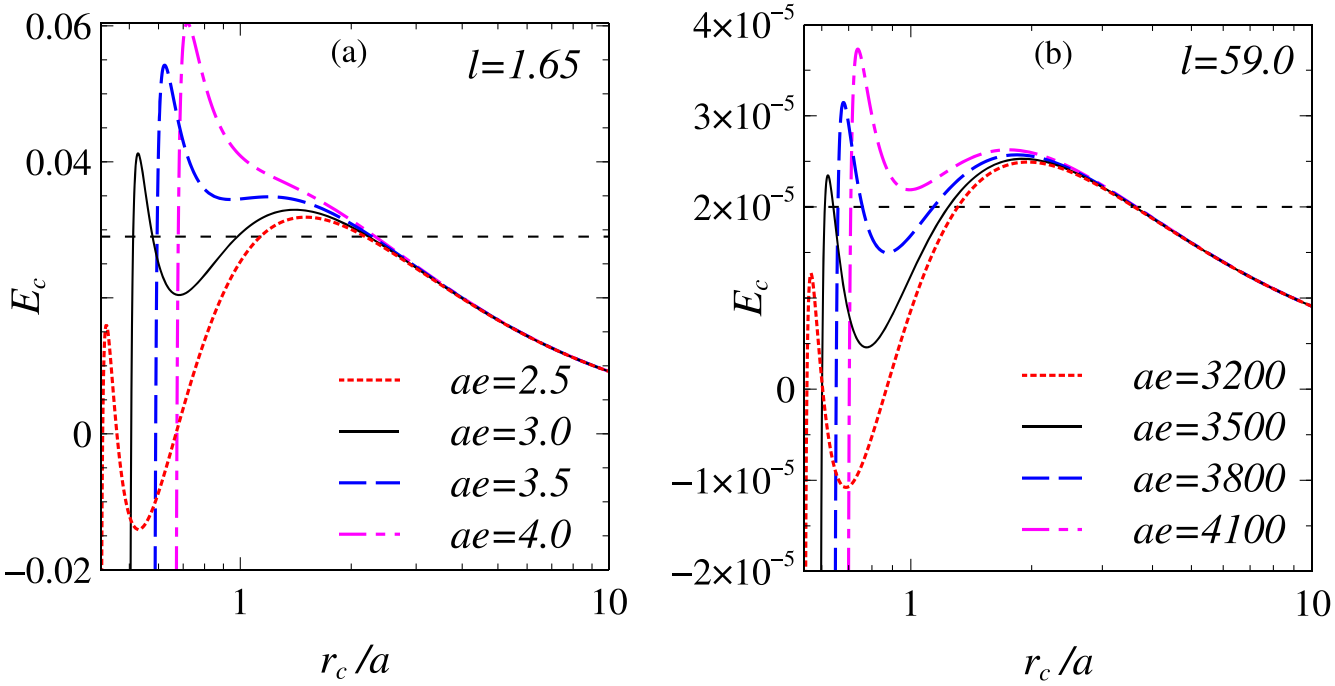

Figure 2. Variation of energy as a function of the critical point location for different values of (semimajor axis(a)×eccentricity(e)). Left panel (a) is for parameters for a typical NS. l is fixed at 1.65. The horizontal line indicates constant energy of 0.029. Right panel (b) is for a typical WD. l is fixed at 59.0. The horizontal line indicates constant energy of 2.0×10^{-5}. Adiabatic index $\gamma = 4/3$. The x-axis values are presenting critical point location in terms of semimajor axis (a) of the compact object where a is assumed to be 6.0 for the NS and 5900.0 for the WD. Keep in mind that only whole value of $a \times e$ affects the dynamics as well as energy, not their individual values.

Table 1
One Set of Values of Different Parameters for Which Shock will Occur for Accretion onto a Typical NS and WD

Central Accretor	a (R_g)	e	l_c	E_c
		0.500	1.650	0.0287–0.0292
NS	6.0	0.500	1.647–1.654	0.0290
		0.503–0.496	1.65	0.0290
		0.600	59.0	$(1.93–2.06)\times10^{-5}$
WD	5900.0	0.600	58.7–59.3	2.00×10^{-5}
		0.585–0.610	59.0	2.00×10^{-5}

Note. Once values of a, e, and l_c are fixed, there is a range of E_c for which shock will occur. This is true for other parameters also. Always there is a range in value of one parameter when other parameters are fixed.

It may arise that the inner critical point lies inside a. In that case, we do the hydrodynamics considering the inner critical point and truncate the accretion flow at $r = a$ to mimic the presence of the surface.

For a transonic flow around an accretor with a hard surface, shock in the accretion flow is almost inevitable because flow has to slow down at the surface (Dhang et al. 2016, 2018). The possibility of formation of the shock is enhanced in an inviscid sub-Keplerian transonic flow if both the outer and inner critical points coexist (Chakrabarti 1989, 1996; Mukhopadhyay 2003). In this work, we do not consider the effects of the presence of the surface and assume there is a sink of mass at the inner boundary. To investigate the formation of shock in principle, we can solve the hydrodynamics from an inner critical point and from an outer critical point and can check whether the shock conditions (Equations (16)–(20)) are satisfied or not in the region between two critical points. However, we follow in a more convenient way to check the possibility of shock, which is by plotting E_c versus $\dot{\mu}_c$ by varying r_c as shown in Figure 3. This is usually called the *swallow-tail* picture (Figure 3). For accretion with shock in the current context, the picture is like the following: matter from a companion that is coming from far away reaches the outer critical point, becomes supersonic, and then due to shock it jumps to the inner critical point branch and finally accretes onto the compact object. In other scenarios, it may be possible to jump to other branches or shock may not happen and matter directly accretes to the compact object. For the present purpose we restrict ourselves to the scenario to jump to the inner critical branch due to the formation of shock.

The swallow-tail picture gives the possible range of energy for which shock may form. In Figure 3, "O" and "I" represent the branch for outer and inner critical point, respectively. We need to find an energy value for which matter can jump from the outer critical branch to the inner critical branch with the necessary condition of increment of entropy as given in Equation (18). This means, as shown in Figure 3, matter will jump from the AB line (branch corresponding to the outer critical point with lower entropy) to the DB line (branch corresponding to the inner critical point with a higher entropy) to make the shock happen. If we draw a constant energy line (which is the energy of the flow), which passes through the AB and DB lines simultaneously, then matter with that energy may jump from a low entropy region to a high entropy region keeping its energy constant. As the probability increases for a y = constant line to intersect AB and DB simultaneously, the probability of the occurrence of shock increases. Keep in mind that it only gives the probability of the shock. Getting a rough

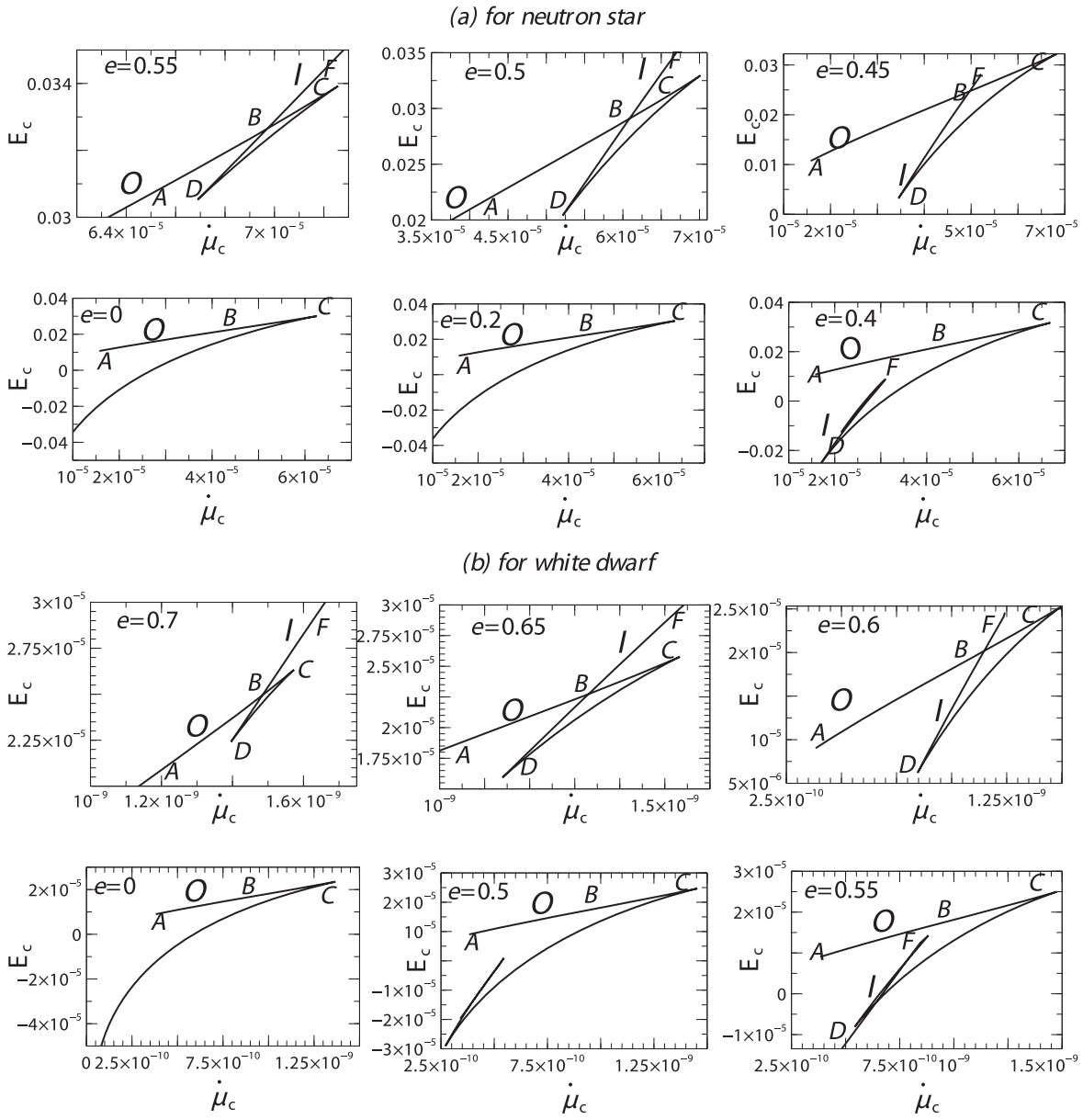

Figure 3. Variation of the possibility of shock with different eccentricity. (a) for an NS case $a = 6.0$ and $l = 1.65$ and (b) for a WD case $a = 5900.0$ and $l = 59.0$ are fixed. ***O*** (AC line) and ***I*** (FD line) represent the outer and inner critical branches, respectively. The range of energy value for which the E_c = constant line passes through both the branches simultaneously gives the possibility of shock formation. It shows that decreasing e increases the possibility of shock up to a certain value for which shock can occur, i.e., until two branches exist simultaneously.

estimate of the energy range with other fixed parameters for the shock, we need to check whether the other condition (Equation (20)) of the shock is satisfied or not.

Figure 3 shows how the eccentricity of the MS changes the possibility of the occurrence of shocks for a typical (a) NS and (b) WD. We found that with decreasing eccentricity keeping the l value fixed, the probability for a y=constant line to cut the AB and DB lines simultaneously increases, which indicates that decreasing eccentricity increases the possibility of formation of shock. However, for the NS (WD) case $e = 0.4$ (0.55) and $l = 1.65$ (59.0), the curve from the inner branch turns back and does not intersect with the outer branch. This returning nature is coming due to the presence of an O type critical point in the innermost region as described earlier. In the rest of the swallow-tail diagrams also, the curve turns back from the inner branch after some value. To keep the picture easy to understand, we have plotted up to that point beyond which returning occurs. When $a = 6.0$ (5900.0), $l = 1.65$ (59.0), for $e = 0.4$ (0.5) or lower values, there is no possible energy value that can intersect with the outer as well as the inner branch. This shows that for the range of e equal to or smaller than a certain value (while other parameters remain fixed), inner and outer critical points cannot exist simultaneously. According to the present scenario of shock formation, shock will not form. From this analysis we can say that decreasing the eccentricity of MS increases the probability of shock as long as the outer and inner critical points exist simultaneously. For slowly rotating nonmagnetic CVs eccentricity is small, which indicates that the occurrence of shock will be more probable unless the inner critical point vanishes. Figure 3 shows for an NS (WD) accretor, flow with specific angular momentum $l = 1.65$ (59.0), accreted onto central

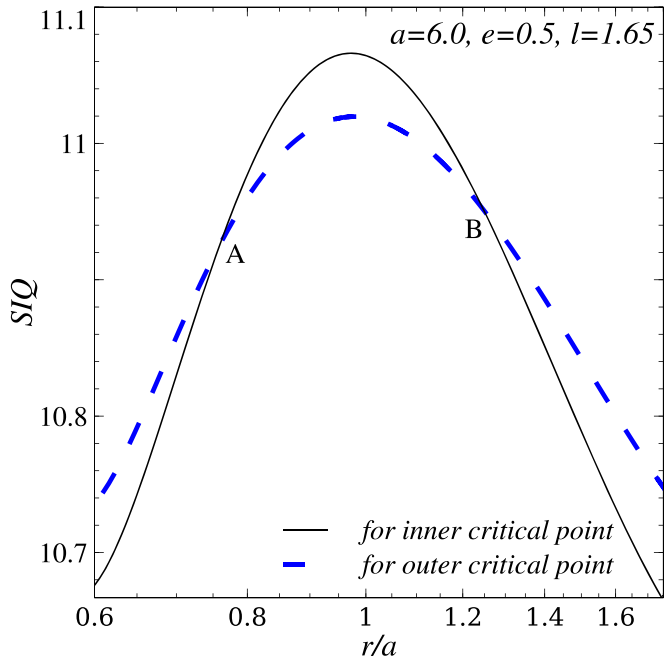

Figure 4. Variation of shock invariant quantity (SIQ) with radial distance for accretion flow with $E_c = 0.0289$ and $l = 1.65$ around the NS. Two curves are for accretion through the outer and inner critical points. The intersection points (A and B) of the two curves indicate the possible shock locations where the inner one (A) is unstable and the outer one (B) represents the actual location of the shock.

accretor having $a = 6.0$ (5900.0) with e in the range 0.45–0.55 (0.55–0.7) is highly probable to make the shock happen.

4. Hydrodynamics around Compact Object

In this section, we investigate the accretion structure around the two different kinds of compact objects, namely, NSs and WDs whose shape can be described by the MS. However, it should be mentioned that while the used Newtonian approach can explain the accretion flow around a WD, GR effects are significant to consider in the case of an accretion disk around an NS. That is why our results presented here for an NS are not realistically accurate. However, we expect that the qualitative nature of the flow will remain same.

4.1. Around an NS

Here, we describe the hydrodynamics of the accretion flow assuming the NS as an MS with typical observed values of mass $1\,M_{\odot}$, $a = 6.0$. We have shown three cases depending on different realistic values of eccentricity (e) of an NS and specific angular momentum (l) of the flow. In perfect combination of e and l, shock forms, but in other cases it disappears.

In Section 3, we see that shock can form for a specific range of parameter space (l, e). A convenient way to check whether shock forms or not is to check the equality in Equation (20). To study it, we simultaneously plot *SIQ* for two branches: when accretion happens through the inner critical point and through the outer critical point. Points of intersection give the locations of shock where flow jumps from the outer critical branch to the inner critical branch. This is shown in Figure 4 for $l = 1.65$ and $e = 0.5$ when the E_c of the flow is 0.0289. Out of two possible shock locations, the inner one is unstable under radial perturbation due to post-shock acceleration. The outer one is stable due to post-shock deceleration (Nakayama 1992; Nobuta & Hanawa 1994). So, the outer intersection point (B) is our desirable shock location. However, even the outer shock location is unstable to non-radial, non-axisymmetric perturbation (Iwakami et al. 2009). These instabilities (oscillations) are invoked to explain different time variabilities (i.e., ejections, quasiperiodic oscillations) in the accreting systems (Molteni et al. 1996, 1999; Bhattacharjee & Chakrabarti 2019).

We consider both shocked and shock-free solutions. This is achieved by solving the equations for $\frac{dv}{dr}$ and $\frac{dc_s}{dr}$ simultaneously for different sets of l and e and keeping $E_c = 0.0289$ fixed. We specify flow parameters at the critical points (where quantities are well determined, see Section 2), and look for the stationary solutions.

Figure 5 shows the radial profiles of the Mach number ($\mathcal{M} = v/c_s$) and sound speed (c_s) for the accretion flow around the NS for $E_c = 0.0289$, $a = 6.0$ for three different sets of parameters: $l = 1.65$, $e = 0.5$; $l = 1.5$, $e = 0.5$; and $l = 1.65$, $e = 0.55$. Although fixing E_c value to 0.0289 gives inner and outer critical points for set ($l = 1.65$, $e = 0.5$), the same energy value gives only the outer critical point for ($l = 1.5$, $e = 0.5$) and ($l = 1.65$, $e = 0.55$), which does not allow the formation of a shock. For the shock solution, the outer and inner critical points occur at $r/a = 2.24$ and 0.58, which makes the shock possible at $r/a = 1.25$. Although, the inner critical point lies within the NS, the flow will remain same as the shock occurs within the flow outside of the NS surface. Therefore, only ($l = 1.65$, $e = 0.5$) gives us shock in advective flow among the three sets. It indicates that accreting matter of the same energy may or may not form shock depending on its specific angular momentum and eccentricity of the central accretor. At the shock, there is a sudden jump in Mach number as well as in sound speed, whereas there is a smooth increase in $\mathcal{M}$ and c_s for other cases as gradually accreted by the NS. Figure 5 is extended until the inner critical point for shock solution. The vertical dotted line indicates the location of the surface where the flow will stop. One set of values of different parameters suitable for shock for an NS having $a = 6.0$ is tabulated in Table 1. Once the values of a, e, and l_c are fixed, there is a range in E_c for which shock will be possible. Similarly, when E_c is fixed, there is a range in values of other parameters for which shock will be possible. However, it is evident as well as worth mentioning that if we can vary all the parameters instead of fixing two as tabulated in Table 1, the range of different parameters becomes quite large for which shock is possible. For accretion onto an NS with $a = 6.0$, shock will be possible by tuning the values of different parameters from range of $e = 0.2$–1.0, $l_c = 1.1$–2.45, and $E_c = 0.005$–0.090. Values of any parameter lying outside of this range will not be able to make the shock happen.

In the literature, the occurrence of shock is possible due to either presence of hard surface of the accretor (Dhang et al. 2016) or the GR correction in the gravitational potential (Chakrabarti 1989, 1996; Mukhopadhyay 2002; Dihingia et al. 2020). The beauty of the MS potential is in the formation of the shock without incorporating any kind of GR effect. Simultaneous formation of the outer as well as the inner critical points allows the formation of shock, which is not possible using the Newtonian potential of a spherical body. To include the GR effect approximately, it is customary to replace the Newtonian potential with the pseudo-Newtonian potential (Paczyński & Wiita 1980) to mimic GR effects on the accretion flow. It

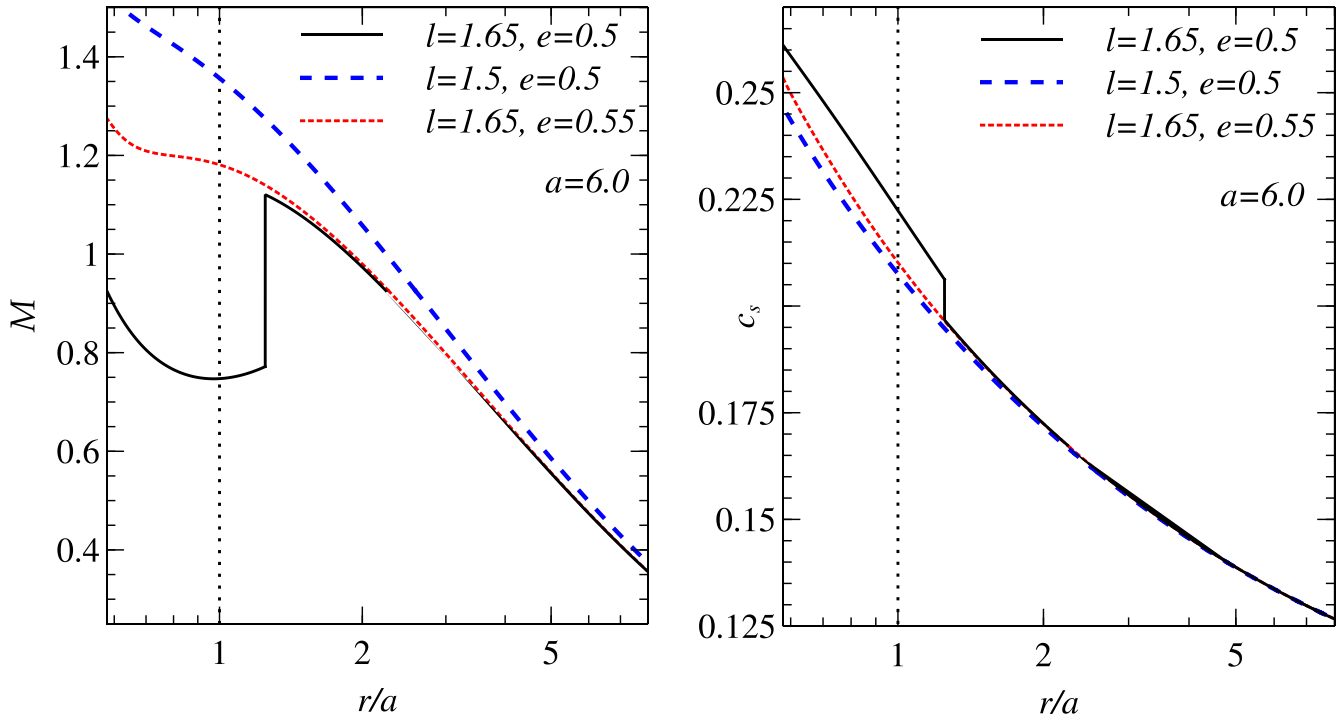

Figure 5. Variation of Mach number($\mathcal{M}$) and sound speed (c_s) with radius with and without formation of shock for different combination of l and e. The x-axis is presenting radius in terms of a. Combination of $l = 1.65$ and $e = 0.5$ gives $r_{c,in}/a = 0.58$ and $r_{c,out}/a = 2.24$ for $E_c = 0.0289$ which makes shock possible at $r_{sh}/a = 1.25$. The plot is extended until inner critical point for shock solution. The vertical dotted line at $r/a = 1$ indicates the surface of the NS.

should also be mentioned that the formation of shock in MS potential is possible even at lower l values compared to what is expected when a pseudo-Newtonian potential is used for the same E_c. In addition to the MS potential effect, inclusion of GR effects for NS accretion will change the properties of the flow and will change the parameter space for our model to be applicable, we expect the qualitative picture, i.e., the change in velocity as well as in sound speed due to shock, the increment in density as well as the enhancement in cooling and change in temperature will remain almost same.

4.2. Around a WD

Here, we describe the hydrodynamics of the accretion flow around a WD that is assumed to be an MS with typical observed values of mass $0.8\,M_\odot$ (Zorotovic & Schreiber 2020) with radius $0.01\,R_\odot$ (Chandrasekhar 1935; Parsons et al. 2017). Conversion of this radius in units of GM/c^2 gives $a \sim 5900$. Here, we have assumed the eccentricity of the WD is 0.6. Balman & Revnivtsev (2012) and Balman (2020) give the transition radii (from standard SSD to advective disk) for quiescent dwarf novae (DNe; as in low state systems) that lie between $(3–10) \times 10^9$ cm (1–6 mHz break frequencies), which in units of R_g becomes around (25,000–85,000) R_g. This indicates the possibility of the presence of advective flow for a sufficiently large radial range, which is required to form the outer as well as the inner critical point simultaneously. As the outer and inner critical points occur simultaneously, it opens up a new possibility of the formation of shock within the flow for WD accretion as the presence of two critical points together is a necessary condition for shock formation!! Though it is not conventional, we used a dimensionless unit to present length scales of the WD.

Here, we followed the same procedure as that for an NS. Due to the larger size of the WD, l also increases largely as Keplerian angular momentum is proportional to $\sqrt{r}$. Also from Equation (14) it is quite clear that the energy at the critical point will reduce drastically due to the reduction in gravitational potential at larger distance. For advective flow with $E_c = 2.0 \times 10^{-5}$, $l = 59.0$ around the WD with $e = 0.6$, there is the simultaneous occurrence of the outer as well as the inner critical point. In Figure 6, we have overplotted the *SIQ* for two cases when accretion happens through the outer as well as the inner critical point. The outer intersection point (B) gives our desired shock location. We have shown radial profiles for $\mathcal{M}$ and c_s for $E_c = 2.0 \times 10^{-5}$ for three different sets: $l = 59.0$, $e = 0.6$; $l = 55.0$, $e = 0.6$; and $l = 59.0$, $e = 0.65$ in Figure 7. Only for ($l = 59.0$, $e = 0.6$) shock occurs, and there is a steep increase in c_s and a decrease in $\mathcal{M}$. For the other two sets, shock disappears and there is gradual increase of $\mathcal{M}$ and c_s as matter goes inward through accretion. As the post-shock region is hotter than the unshocked flow, the post-shock region will be puffed up and inflated as shown in Figure 1 of Chakrabarti & Titarchuk (1995). For the shock solution, the outer and inner critical points occur at $r/a = 3.6$ and 0.65, which makes the shock possible at $r/a = 1.86$. Although, the inner critical point lies within the WD, the flow will remain undisturbed as the shock occurs within the flow outside of WD surface. This indicates again that shock can occur for only a certain range of parameters. For a specific value of E_c, only a certain range of l and ae values will result in shock. One set of values of different parameters that makes the shock possible for accretion onto a WD with $a = 5900.0$ is tabulated in Table 1. However, it is evident as well as worth mentioning that if we can vary all the parameters instead of fixing two as tabulated in Table 1, the range of different parameters becomes quite large for which shock is possible. For accretion onto a WD with $a = 5900.0$,

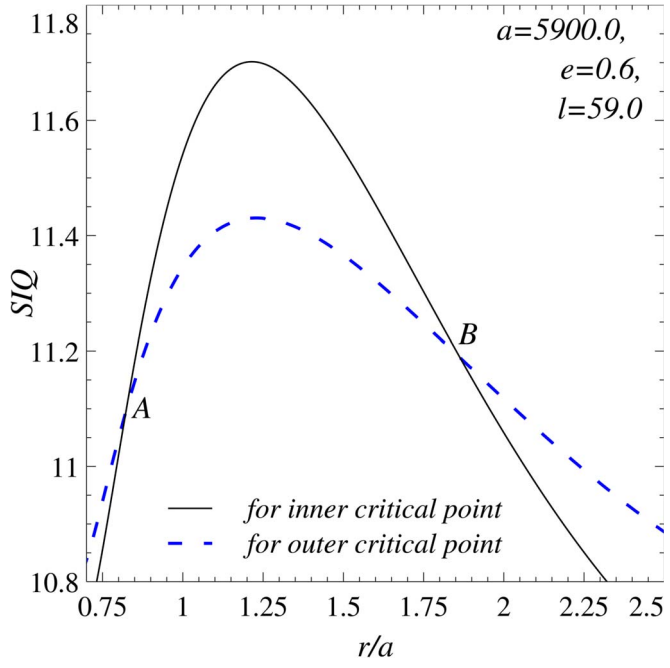

Figure 6. Variation of shock invariant quantity (SIQ) with radial distance for accretion flow with $E_c = 2.0 \times 10^{-5}$ and $l = 59.0$ around the WD. Two curves are for accretion through the outer and inner critical points. The intersection points (A and B) of the two curves indicate the possible shock locations where the inner one (A) is unstable and the outer one (B) represents the actual location of the shock.

shock will be possible by tuning the values of different parameters from the range of $e = 0.2$–1.0, $l_c = 32.0$–76.0 and $E_c = (1$–$8) \times 10^{-5}$. Values of any parameter lying outside of this range will not be able to make the shock happen. Figure 7 is extended until the inner critical point for shock solution. The vertical dotted line indicates the location of the surface where the flow will stop. The angular momentum value increases in comparison with the NS as the value of a increases. Larger angular momentum is required to have an effect at a larger distance from the central accretor.

Here, the result is more robust as hardly any GR effect will come into the picture and also the formation of shock is not possible within the accretion flow in the Newtonian potential of a spherical body. So, new phenomena arise only due to deformation of the shape of the accreting WD. To the best of our knowledge we suppose, for the first time we are reporting this kind of shock formation for WD accretion. As the formation of sub-Keplerian advective flow up to the surface of the WD is possible for nonmagnetic CVs, only spinning of the WD should be sufficient to deform it. This is further justified in the discussion section from an observational point of view.

5. Discussion

We have discussed the hydrodynamics around an NS, as well as around a WD. However, we must emphasize that the Newtonian description of the hydrodynamics is more suitable to describe the accretion physics around a WD compared to that around an NS, where GR effects are important. Our proposed model is specifically applicable to nonmagnetic CVs where stellar magnetic field has a negligible effect on the accretion, unlike polars or intermediate polars (for a review see Mukai 2017). Observations reveal more than 70% of the CVs are nonmagnetic (Ferrario et al. 2015, 2020).

Nonmagnetic CVs are broadly classified into nova-likes (NLs) and DNe. NLs spend most of their time in a high state (i.e., high mass accretion rate) with UV emission predominantly originating from the disk (La Dous 1991), while DNe are observed mostly in the quiescent state (low mass accretion rate) (Hack & La Dous 1993). However, DNe show periodic outbursts (when mass accretion rate rises) with disk-dominated optical and UV emission.

5.1. Accretion with Suitable Parameters Will Give Rise to Shocks

Figure 1 and Figure 2 show that there is a specific range of l_c and ae values for which simultaneous occurrence of two X-type critical points is possible for the accretion flow onto an NS and a WD. In the presence of two X-type critical points, shock becomes possible. Once l_c and ae are fixed, from the swallow-tail diagram (Figure 3) we can estimate the energy range for which shock is possible. And finally matching the shock invariant quantity (Equation (20)), we find the exact energy of the flow that is required to make the shock possible for a suitable l_c and ae. One set of values of different parameters suitable for shock for an NS having $a = 6.0$ and for a WD having $a = 5900.0$ is tabulated in Table 1. Once values of a, e, and l_c are fixed, there is a range of E_c for which shock will occur. This is true for other parameters also. There is always a range in value of one parameter when other parameters are fixed. It is quite encouraging that shock is possible for a wide range of eccentricity ($e = 0.2$–1.0) of an NS and a WD. Therefore, in summary, accretion flow having suitable specific angular momentum and energy (here l_c and E_c mimics these values due to the inviscid nature of the flow) will make shock when accreted to a suitable accretor (suitable ae value). If conditions are suitable (appropriate values of parameters for the shock), a shocked solution is more likely to happen in the course of the accretion process instead of a shock-free solution due to the nature of entropy, which preferably increases.

5.2. Is Sufficient Deformation of a WD Possible?

Before drawing any connection of the described model to the observed phenomena in nonmagnetic CVs, we would like to check the justification of the considered stellar deformation quantified by the parameter e. We find that shock is possible for a wide range of eccentricity ($e = 0.2$–1.0) of an NS and a WD if values of other parameters are chosen suitably. As the e of the accretor decreases, the required l_c for the shock also decreases, i.e., for a accretor that is more spherical (lower e value, $e = 0$ for a sphere), more sub-Keplerian flow (lesser angular momentum) is required to make the shock possible. Within the limited observed samples it has been estimated that the spin frequency Ω_* of many nonmagnetic CVs lies in the range (0.01–0.3) Ω_K (Sion 1999; Godon et al. 2012), where Ω_K is the Keplerian angular velocity at the surface of the WD. Such values of Ω_* are good enough to generate the eccentricity e ($\sim$0.2–0.4) (equation (7.3.18) of Chandrasekhar 1969; Shapiro & Teukolsky 1983) and even more oblate with low density of the spheroid. The possibility of shock for any $e \geqslant 0.2$ (with appropriate l_c) indicates the applicability of our model for the WDs with observed rotational frequencies.

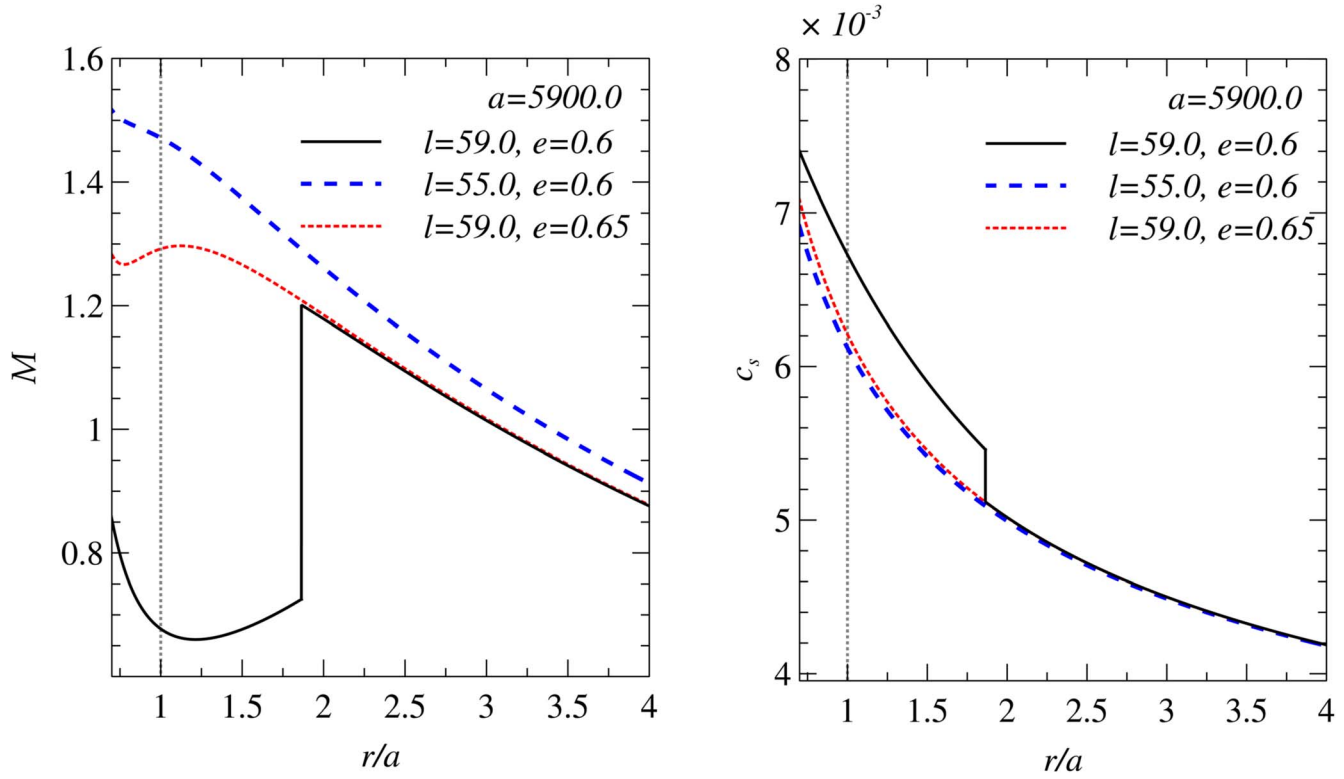

Figure 7. Variation of Mach number ($\mathcal{M}$) and sound speed (c_s) with radius the same as in Figure 5 but here the compact object is a WD. Here, the combination of $l = 59.0$ and $e = 0.6$ gives $r_{c,in}/a = 0.65$ and $r_{c,out}/a = 3.6$ (~0.00017 au) for $E_c = 2.0 \times 10^{-5}$, which makes shock possible at $r_{sh}/a = 1.86$. The plot is extended until the inner critical point for shock solution. The vertical dotted line $r/a = 1$ indicates the surface of the WD.

5.3. Advective Flows in CVs

The UV spectra from the disk-dominated nonmagnetic CVs (high state CVs) are generally modeled using the standard disk model (Wade & Hubeny 1998). However, a significant fraction of the theoretical spectra were found to be too blue compared to the observed UV spectra (Linnell et al. 2005; Puebla et al. 2007; Godon et al. 2017).

Because of the presence of the hard surface in the WD, a boundary layer (BL) is expected to form between the stellar surface and the Keplerian disk (Pringle 1981; Frank et al. 2002). The BL is predicted to be optically thick and to emit soft X-rays during high accretion states (high states in NLs and outbursts in DNe) (Narayan & Popham 1993; Popham& Narayan 1995), while hard X-ray is expected from an optically thin BL region during quiescence (Pringle & Savonije 1979; Narayan & Popham 1993). Although hard X-ray is observed in quiescent sources as expected (Szkody et al. 2002; Pandel et al. 2005), sources also exhibit optically thin hard X-ray emission in the high accretion states (van Teeseling et al. 1996; Balman et al. 2014; Balman 2020).

Inadequacy of the standard disk model in explaining observed UV spectra in high states (Puebla et al. 2007; Godon et al. 2017) and presence of the optically thin hard X-rays in low (quiescent DNe) as well as in high accretion states as in NLs and outbursting DNe, is best explained in the context of radiatively inefficient hot advective accretion flows (ADAF-like) that exist in nonmagnetic CVs (Balman & Revnivtsev 2012; Balman 2020 and references therein). It is detected that an outer optically thick Keplerian disk is truncated to optically thin hot advective flow in the quiescent and outbursting DNe (Balman 2020 see Section 3). The outer Keplerian disk moves inward as mass accretion rate increases during the outbursts (Balman & Revnivtsev 2012; Balman 2019). Therefore a natural expectation is that a hot advective flow is supposed to exist both in low and in high accretion states of nonmagnetic CVs.

5.4. Plausible Connection of Shock in Advective Flows to Observables

The spectra from accreting WDs used to be modeled as multi-temperature isobaric cooling flow (power law and/or Bremsstrahlung) (mkcflow/CEVMKL in XSPEC or using two/more MEKAL components) (Mukai 2017 and references therein). In this model, the emission measure at each temperature is proportional to the time the cooling gas remains at that temperature. For most of the accreting WDs, the multi-MEKAL component significantly improves the spectra in comparison with a single component (Mauche & Mukai 2002; Pandel et al. 2005; Balman et al. 2014). Moreover, the presence of nonequilibrium ionization conditions of the plasma and the emission lines (N, O, Ne, Mg, Si, and Fe) are detected for several nonmagnetic CVs in X-rays (Schlegel et al. 2014; Balman 2020); however, this is not explored in the present form of our model.

One of the characteristic property of advective flows is that the inward flow velocity increases very rapidly as it approaches the central accretor (Chakrabarti 1989; Narayan & Yi 1994; Chakrabarti 1996). The rapid increase in radial velocity also seen in the shock-free solutions denoted by the short and long dashed curves in Figures 5 and 7. Large radial velocity close to the accretor gives very little time to the flow for emission. The occurrence of shock in the advective flow (as discussed in

Section 4) leads to the rise in temperature ($\sim c_s^2$) as well as an increase in density in the post-shock region. In addition, in the post-shock flow, the radial velocity decreases, leading to a longer time span of the flow at higher temperatures. The optically thin radiatively inefficient advective flow in nonmagnetic CVs will give rise to radiation in the hard X-rays as they approach the central WD. The occurrence of the shock will alter the intensity as well as the hardness of the spectra, which can also explain the variation of the efficiency of X-ray luminosity at different accretion rates (see Balman 2020, Section 2.3, 3 for a discussion). Hard X-rays are mainly observed in quiescent as well as in high accretion rate CVs and most related accreting WD systems (van Teeseling et al. 1996; Szkody et al. 2002; Pandel et al. 2005; Balman et al. 2014; Balman 2020). On a note of caution, as the location of the truncation radius moves closer to the central accretor in high accretion states of nonmagnetic CVs, leaving a small radial range for the advective flow to make the shock happen, the occurrence of shock will become less probable.

5.5. Caveats

In this work, we have analyzed the sonic point formation, shocks in a steady inviscid sub-Keplerian advective flow and and the related astrophysical implications. Due to the inviscid nature of the flow, the energy and the specific angular momentum of the flow at the critical points (E_c and l_c) becomes the energy and angular momentum of the flow at all radial distances. Energy and specific angular momentum remain constant throughout the flow. It cannot be true in reality.

The specific angular momentum value we are using for the formation of shock in WD accretion is $l_c = 59$. At the WD surface, the ratio of specific angular momentum and Keplerian angular momentum becomes $\sim$0.77. Though it might be very low keeping the Keplerian disk in mind, it is customary to assume such low angular momentum value to do the analyses we have done in the sub-Keplerian advective flow (Chakrabarti 1989; Das et al. 2001; Mukhopadhyay 2003; Palit et al. 2019; Dihingia et al. 2020).

To solve the dynamics, we have used polytropic equation of state of the flow instead of solving energy equation. Also we have not incorporated any radiative cooling in the model. Therefore, it is not possible to comment on the actual spectra or luminosity generated due to the flow. In the near future, we would like to do time-dependent calculations of the magnetized advective flow, including radiative cooling and by solving the energy equation explicitly.

6. Summary

In this paper, we have studied the hydrodynamics of an optically thin advective flow around a deformed (from spherical shape) compact object that has a finite surface, e.g., an NS or a WD. We treat the deformed star as an MS. Treating the compact object as an MS opens up a new possibility for the formation of Rankine–Hugoniot shock, which is not possible for accretion around a spherical accretor without considering GR effects or effects of the hard surface of the accretor. To the best of our knowledge, for the first time we are reporting the possibility of the occurrence of a shock in the radiatively inefficient hot advective flow around a WD. As far as we are concerned to understand the flow hydrodynamics around the nonmagnetic CVs, our findings are robust as flow around a WD hardly deviates from the Newtonian regime. Although we have assumed inviscid flow and have not included radiative cooling for this preliminary study, we believe our findings will remain the same qualitatively. We propose that some observational features, e.g., high significance of fitting the spectra with multi-temperature plasma models rather than single-temperature models, and variable efficiency of X-ray emission (X-ray luminosity in comparison with optical and UV luminosity of the disk) in nonmagnetic CVs can be explained by the presence of shock in the sub-Keplerian advective flow.

We would like to thank Banibrata Mukhopadhyay, Vikram Rana, and Tushar Mondal for their useful discussion. We are very much thankful to the anonymous referee for insightful suggestions and referring to appropriate references. This work is partly supported by the fund of DST INSPIRE fellowship belonging to SRD.

References

Abramowicz, M. A., Czerny, B., Lasota, J. P., & Szuszkiewicz, E. 1988, ApJ, 332, 646
Amsterdamski, P., Bulik, T., Gondek-Rosińska, D., & Kluźniak, W. 2002, A&A, 381, L21
Balman, Ş. 2019, AN, 340, 296
Balman, Ş. 2020, AdSpR, 66, 1097
Balman, Ş., Godon, P., & Sion, E. M. 2014, ApJ, 794, 84
Balman, Ş., & Revnivtsev, M. 2012, A&A, 546, A112
Bhattacharjee, A., & Chakrabarti, S. K. 2019, ApJ, 873, 119
Bondi, H. 1952, MNRAS, 112, 195
Chakrabarti, S., & Titarchuk, L. G. 1995, ApJ, 455, 623
Chakrabarti, S. K. 1989, ApJ, 347, 365
Chakrabarti, S. K. 1996, ApJ, 464, 664
Chakrabarti, S. K. 1990, Theory of Transonic Astrophysical Flows (Singapore: World Scientific Publishing Co)
Chandrasekhar, S. 1935, MNRAS, 95, 207
Chandrasekhar, S. 1969, Ellipsoidal Figures of Equilibrium (New Haven, CT: Yale Univ. Press)
Chatterjee, A., Chakrabarti, S. K., Ghosh, H., & Garain, S. K. 2018, MNRAS, 478, 3356
Das, S., Chattopadhyay, I., Chakrabarti, S. I. K., et al. 2001, ApJ, 557, 983
Das, U., & Mukhopadhyay, B. 2015, JCAP, 2015, 016
Dhang, P., Sharma, P., & Mukhopadhyay, B. 2016, MNRAS, 461, 2426
Dhang, P., Sharma, P., & Mukhopadhyay, B. 2018, MNRAS, 476, 3310
Dihingia, I. K., Das, S., Prabhakar, G., & Mandal, S. 2020, MNRAS, 496, 3043
Ferrario, L., de Martino, D., & Gänsicke, B. T. 2015, SSRv, 191, 111
Ferrario, L., Wickramasinghe, D., & Kawka, A. 2020, AdSpR, 66, 1025
Frank, J., King, A., & Raine, D. J. 2002, Accretion Power in Astrophysics, Vol. 398 (3rd ed.; Cambridge: Cambridge Univ. Press)
Godon, P., Sion, E. M., Balman, Ş., & Blair, W. P. 2017, ApJ, 846, 52
Godon, P., Sion, E. M., Levay, K., et al. 2012, ApJS, 203, 29
Hack, M., & La Dous, C. 1993, Cataclysmic Variables and Related Objects, Vol. 507 (Washington, DC: NASA)
Haskell, B., Samuelsson, L., Glampedakis, K., & Andersson, N. 2008, MNRAS, 385, 531
Iwakami, W., Kotake, K., Ohnishi, N., Yamada, S., & Sawada, K. 2009, ApJ, 700, 232
Kluźniak, W., & Rosińska, D. 2013, MNRAS, 434, 2825
Komatsu, H., Eriguchi, Y., & Hachisu, I. 1989, MNRAS, 237, 355
La Dous, C. 1991, A&A, 252, 100
Landau, L. 1987, Fluid Mechanics: Landau and Lifshitz Course of Theoretical Physics, Vol. 6 (Oxford: Pergamon Press)
Linnell, A. P., Szkody, P., Gänsicke, B., et al. 2005, ApJ, 624, 923
Mauche, C. W., & Mukai, K. 2002, ApJL, 566, L33
Medvedev, M. V., & Menou, K. 2002, ApJL, 565, L39
Mishra, B., & Vaidya, B. 2015, MNRAS, 447, 1154
Molteni, D., Sponholz, H., & Chakrabarti, S. K. 1996, ApJ, 457, 805
Molteni, D., Tóth, G., & Kuznetsov, O. A. 1999, ApJ, 516, 411
Mukai, K. 2017, PASP, 129, 062001
Mukhopadhyay, B. 2002, ApJ, 581, 427

Mukhopadhyay, B. 2003, ApJ, 586, 1268
Nakayama, K. 1992, MNRAS, 259, 259
Narayan, R., Mahadevan, R., & Quataert, E. 1998, in Theory of Black Hole Accretion Disks, ed. M. A. Abramowicz, G. Björnsson, & J. E. Pringle (Cambridge: Cambridge Univ. Press), 148
Narayan, R., & Popham, R. 1993, Natur, 362, 820
Narayan, R., & Yi, I. 1994, ApJL, 428, L13
Narayan, R., & Yi, I. 1995, ApJ, 452, 710
Nobuta, K., & Hanawa, T. 1994, PASJ, 46, 257
Novikov, I. D., & Thorne, K. S. 1973, in Black Holes (Les Astres Occlus), ed. C. Dewitt & B. S. Dewitt (New York: Gordon & Breach), 343
Ostriker, J. P., & Bodenheimer, P. 1968, ApJ, 151, 1089
Ostriker, J. P., & Hartwick, F. D. A. 1968, ApJ, 153, 797
Paczyński, B., & Wiita, P. J. 1980, A&A, 88, 23
Palit, I., Janiuk, A., & Sukova, P. 2019, MNRAS, 487, 755
Pandel, D., Córdova, F. A., Mason, K. O., & Priedhorsky, W. C. 2005, ApJ, 626, 396
Parsons, S. G., Gänsicke, B. T., Marsh, T. R., et al. 2017, MNRAS, 470, 4473
Popham, R., & Narayan, R. 1995, ApJ, 442, 337
Pringle, J. E. 1981, ARA&A, 19, 137
Pringle, J. E., & Savonije, G. J. 1979, MNRAS, 187, 777
Puebla, R. E., Diaz, M. P., & Hubeny, I. 2007, AJ, 134, 1923
Rajesh, S. R., & Mukhopadhyay, B. 2010, MNRAS, 402, 961
Schlegel, E. M., Shipley, H. V., Rana, V. R., Barrett, P. E., & Singh, K. P. 2014, ApJ, 797, 38
Shakura, N. I., & Sunyaev, R. A. 1973, A&A, 24, 337
Shapiro, S. L., & Teukolsky, S. A. 1983, Black Holes, White Dwarfs, and Neutron Stars: The Physics of Compact Objects (New York: Wiley-Interscience)
Sion, E. M. 1999, PASP, 111, 532
Subramanian, S., & Mukhopadhyay, B. 2015, MNRAS, 454, 752
Szkody, P., Nishikida, K., Raymond, J. C., et al. 2002, ApJ, 574, 942
van Teeseling, A., Beuermann, K., & Verbunt, F. 1996, A&A, 315, 467
Wade, R. A., & Hubeny, I. 1998, ApJ, 509, 350
Yuan, F., Cui, W., & Narayan, R. 2005, ApJ, 620, 905
Zorotovic, M., & Schreiber, M. R. 2020, AdSpR, 66, 1080